

High-Power CMUTs: Design and Experimental Verification

F. Yalçın Yamaner, *Member, IEEE*, Selim Olçum, *Member, IEEE*,
H. Kağan Oğuz, *Student Member, IEEE*, Ayhan Bozkurt, *Member, IEEE*,
Hayrettin Köymen, *Senior Member, IEEE*, and Abdullah Atalar, *Fellow, IEEE*

Abstract—Capacitive micromachined ultrasonic transducers (CMUTs) have great potential to compete with piezoelectric transducers in high-power applications. As the output pressures increase, nonlinearity of CMUT must be reconsidered and optimization is required to reduce harmonic distortions. In this paper, we describe a design approach in which uncollapsed CMUT array elements are sized so as to operate at the maximum radiation impedance and have gap heights such that the generated electrostatic force can sustain a plate displacement with full swing at the given drive amplitude. The proposed design enables high output pressures and low harmonic distortions at the output. An equivalent circuit model of the array is used that accurately simulates the uncollapsed mode of operation. The model facilitates the design of CMUT parameters for high-pressure output, without the intensive need for computationally involved FEM tools. The optimized design requires a relatively thick plate compared with a conventional CMUT plate. Thus, we used a silicon wafer as the CMUT plate. The fabrication process involves an anodic bonding process for bonding the silicon plate with the glass substrate. To eliminate the bias voltage, which may cause charging problems, the CMUT array is driven with large continuous wave signals at half of the resonant frequency. The fabricated arrays are tested in an oil tank by applying a 125-V peak 5-cycle burst sinusoidal signal at 1.44 MHz. The applied voltage is increased until the plate is about to touch the bottom electrode to get the maximum peak displacement. The observed pressure is about 1.8 MPa with -28 dBc second harmonic at the surface of the array.

I. INTRODUCTION

CAPACITIVE micromachined ultrasonic transducers (CMUTs) are used to generate and detect ultrasound [1], by utilizing a microfabricated suspended moving plate for the transduction. Recent improvements in CMUT designs [2]–[4] and operating methods [5], [6] and advances in the fabrication methodology [7]–[9] demonstrate promising results which make the CMUT technology a strong candidate for different ultrasound applications [10]–[15].

Manuscript received October 18, 2011; accepted March 26, 2012. This work was supported by the Scientific and Technological Research Council of Turkey (TUBITAK) under project grant 107T921 and 110E216.

F. Y. Yamaner and A. Bozkurt are with the Electronics Engineering Department, Sabanci University, Istanbul, Turkey (e-mail: yalcin@sabanciuniv.edu).

S. Olçum was with and H. K. Oğuz, H. Köymen, and A. Atalar are with the Electrical and Electronics Engineering Department, Bilkent University, Ankara, Turkey.

S. Olçum is now with the Department of Biological Engineering, Massachusetts Institute of Technology, Cambridge, MA.

DOI <http://dx.doi.org/10.1109/TUFFC.2012.2318>

High-intensity focused ultrasound (HIFU) is a high-power applications in which sound waves are focused on abnormal tissue and destroy it by delivering high energy [16]. Recently, it has been demonstrated that CMUTs can be used as HIFU transducers [17], [18]. CMUTs can be fabricated using silicon as a membrane material which has high thermal conductivity and can eliminate the requirement of a cooling system [19]. The monolithic integration of imaging and HIFU CMUTs has been realized and tested [20]. Magnetic resonance (MR) compatible CMUTs with different plate topologies have been fabricated, and it has been shown that the output pressures can be increased by using piston-shaped plates [21]. CMUTs with dual electrodes enable leveraged bending and increase the total displacement of the plate in the transmit operation [3], [22]. Using side electrodes, it is possible to move the plate in a wider displacement range without collapsing; however, the voltages required for bending the plate are higher when compared with a CMUT with full electrode coverage.

In this paper, we propose a methodology to design and operate CMUTs to generate single tone, high-amplitude pressure waves with low harmonic content. We employ an equivalent circuit that was developed in [23]. We excite the CMUT at half of the resonance frequency of the plate without a dc bias voltage to reduce the harmonic content and the effect of the charge trapping within the thin dielectric layer between the CMUT electrodes.

II. NONLINEAR EQUIVALENT CIRCUIT MODEL

The electrode coverage of a CMUT plays a major role in both transmit and receive operations. Usually, CMUTs are designed with half electrode coverage for the receive mode to optimize the receive sensitivity [24]. However a higher transmit sensitivity is possible with full electrode coverage, because a larger electrode increases the total electrical force acting on the plate. Therefore, we choose to utilize a CMUT structure with full electrode coverage to generate the maximum pressure for a given voltage. Fig. 1 shows a representative cross section of a circular CMUT cell.

Although a suspended circular plate is modeled by a linear spring, CMUT operation is not linear because of the nonlinear dependence of the electrical force on the plate position. In this work, we use the nonlinear equivalent circuit model shown in Fig. 2 [23], [25].

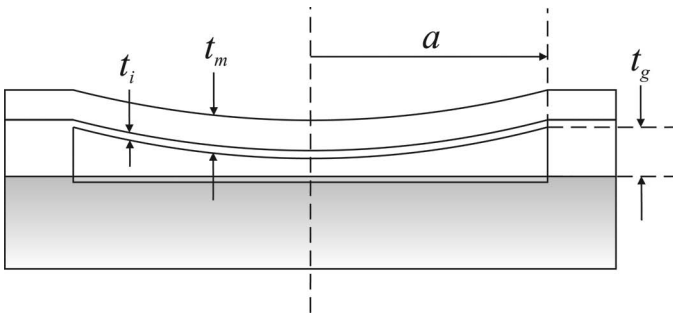


Fig. 1. Representative cross section of a circular plate with radius a , thickness t_m , and gap height of t_g . The top electrode is the high-conductivity silicon wafer. t_i is the thickness of the insulation layer beneath the silicon wafer. The bottom electrode is a gold layer embedded in the substrate.

A. Circuit Model Components

In the electrical part of the equivalent circuit, C_0 is the shunt input capacitance of the CMUT, i_c is the non-linear component of the capacitive current, and i_{vel} is the motion-induced current that accounts for the movement of the plate. The mechanical part of the circuit is on the right-hand side. The electrical attraction force, f_R , and the force exerted by the atmospheric pressure, F_b are represented by voltage sources. The mass and the compliance of the plate are represented by an inductor, L_{Rm} , and a capacitance, C_{Rm} , respectively. The expressions for calculating the circuit parameters can be found in the Appendix. The radiation impedance of the medium is modeled by an impedance, Z_{RR} , terminating the acoustic port of the circuit. The parameter N represents the number of cells in an array and provides scaling to the equivalent circuit. The behavioral current and voltage sources in the circuit require the instantaneous peak displacement of the plate, x_p , as a parameter; x_p is calculated by a small subcircuit depicted separately at the bottom of Fig. 2. The subcircuit calculates the displacement by dividing the restoring force of the plate, F_{Rm} , by the plate compliance.

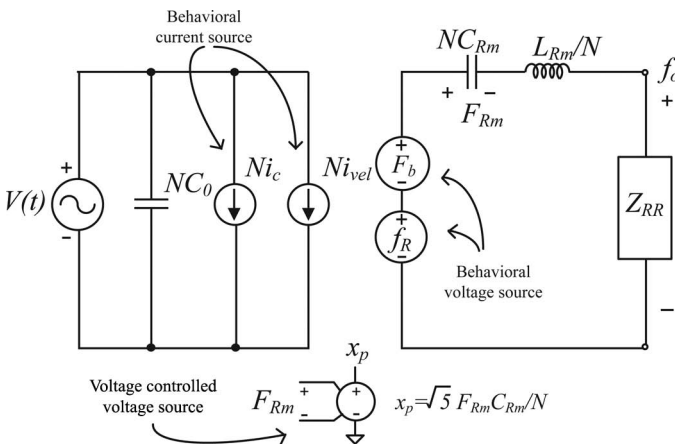


Fig. 2. Electrical circuit model of a capacitive micromachined ultrasonic transducer (CMUT) array driven by voltage source $V(t)$. The radiation impedance, Z_R , is modeled by an RLC circuit. N represents the number of cells in the array.

TABLE I. PLATE MATERIAL PROPERTIES USED IN SIMULATIONS.

Young's modulus of Si, Y_0	1.3e11
Density of Si, ρ	2330
Poisson ratio of Si, σ	0.28
Permittivity of SiO_2 , ϵ_i	3.9
Density of water, ρ_0	1000 kg/m ³
Speed of sound in water, c	1500 m/s

B. Thick Plates

The expressions for calculating the force and compliance relations assume a thin plate approximation [23], [25]. Using this approximation, the first series resonance frequency of the plate can be calculated precisely for $t_m/a < 0.1$ [9]. If the plate is not thin, the accuracy of the model degrades. Using finite element modeling (FEM) simulation results for thick plates, a correction factor is applied to C_{Rm} :

$$C'_{Rm} = C_{Rm} \left(1.019 + 5.005 \left(\frac{t_m}{a} \right)^{1.981} \right) \quad \text{for } t_m/a < 0.8. \quad (1)$$

With this modification, the resonance frequency determined from the circuit model is in good agreement with FEM simulation results. The model loses its accuracy for frequencies close to the antiresonance frequency, because a first-order LC circuit is inadequate to model high-order modes of a CMUT plate [26]. Table I lists the material properties used in the simulations.

In Fig. 3, we test the accuracy of the model in static conditions for thick plates by comparing static deflections obtained from FEM and SPICE simulations for different bias voltages.

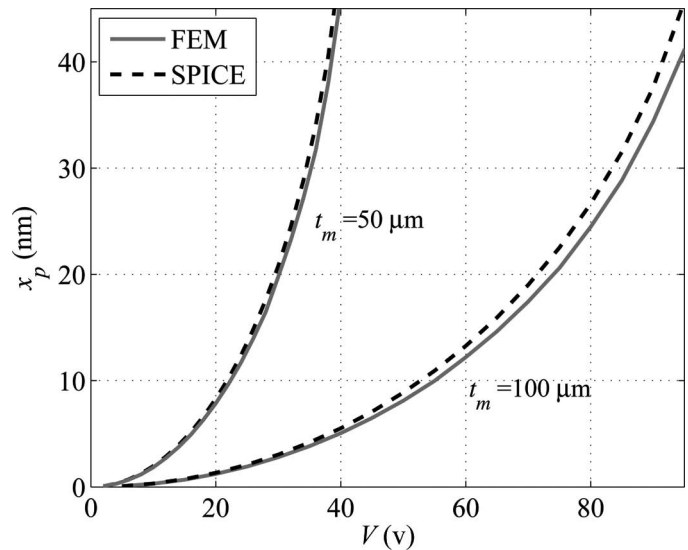


Fig. 3. Comparison of the static deflections obtained from finite element modeling (FEM) and the SPICE model for thick plates ($a = 300 \mu\text{m}$, $t_g = 100 \text{ nm}$, $t_i = 200 \text{ nm}$).

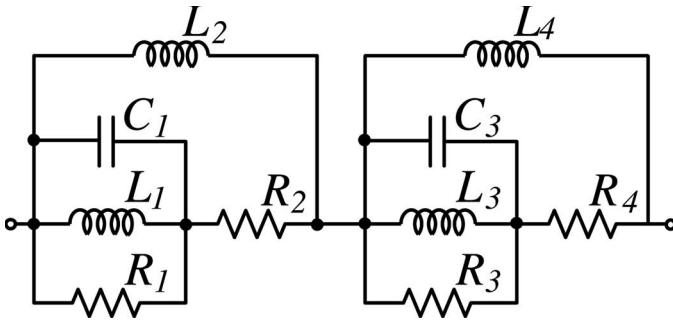


Fig. 4. *RLC* model for the radiation impedance of a capacitive micromachined ultrasonic transducer (CMUT) array.

C. Radiation Impedance

The radiation impedances of a CMUT cell and an array of CMUTs were calculated in [27] for conventional mode of operation. The radiation impedance is a complex quantity and a strong function of the ka product, where k is the wavenumber. For an accurate simulation in SPICE, the radiation impedance can be modeled by using an *RLC* network (Fig. 4) as in [28]. The component values are defined in terms of the plate radius, a , the velocity of the sound in the medium, c , the density of the immersion medium, ρ_0 , cell-to-cell separation, d , and the number of cells in the array, N . The component values for configurations with different numbers of cells, as shown in Fig. 5, are given in Table II.

The accuracy of the network is demonstrated in Fig. 6 for $N = 1$ and $N = 7$. Using the parameters in Table II, the network can be used to accurately model the radiation impedance of an array with 19 CMUT cells, as well.

D. Circuit Simulations

The equivalent circuit in Fig. 2 is simulated with LTSpice (Linear Technology, Milpitas, CA; <http://www.linear.com/designtools/software>). Each circuit component

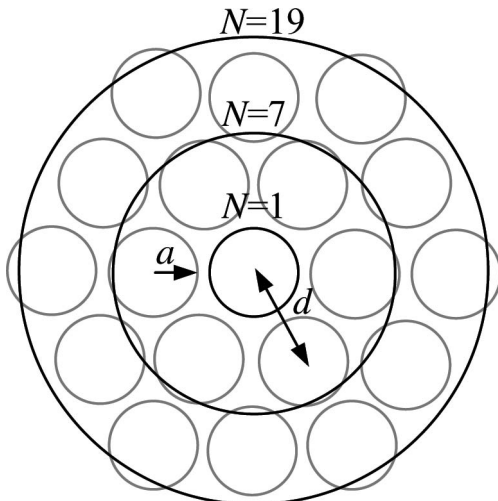


Fig. 5. Configuration of the capacitive micromachined ultrasonic transducer (CMUT) array for different number of cells.

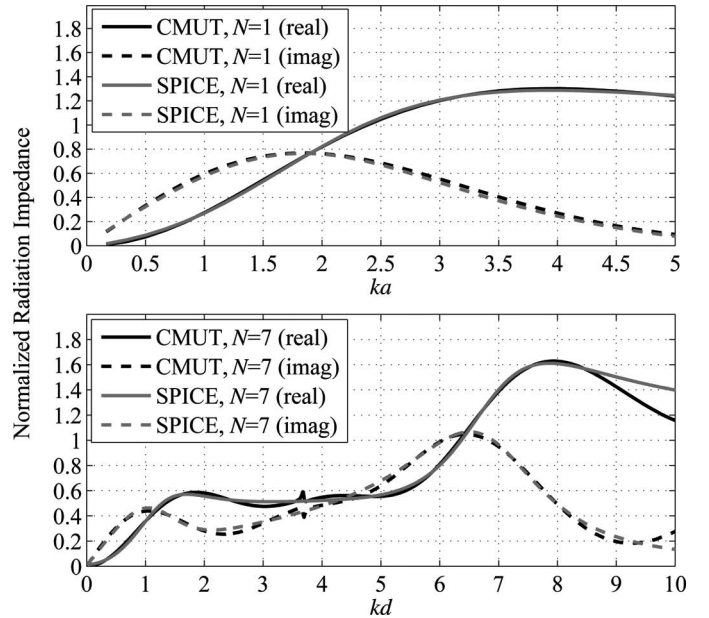


Fig. 6. Comparison of the normalized radiation resistance and reactance of (top) a single capacitive micromachined ultrasonic transducer (CMUT) cell and (bottom) a CMUT array of 7 cells with the *RLC* model and actual values. (The normalization constant is $\pi a^2 \rho_0 c / N$, $d = 2a$.)

in the model is defined parametrically in terms of the CMUT geometry and the material properties. The performance of the equivalent circuit is tested by simulating an excitation of a 2-cycle 95-V peak sinusoidal burst at half of the resonance frequency of a CMUT cell. The center displacement of the plate is compared with the FEM simulation results in Fig. 7. The details of FEM model can be found in [3].

The surface pressure can be calculated by dividing the force across the radiation impedance by the surface area of the CMUT cell. Output power can be calculated by taking average of the product of force and velocity over the plate surface.

III. CMUT DESIGN

A. Excitation at Half of the Operating Frequency

Conventionally, transmitting CMUTs are operated with a bias voltage, which may degrade the device performance

TABLE II. COMPONENT VALUES FOR THE RADIATION IMPEDANCE MODEL WITH DIFFERENT NUMBERS OF CELLS IN THE ARRAY.

N	1	7	19
R_1/R_n	0.64	0.39	0.48
L_1/R_n	0.54 a/c	0.55 d/c	1.2 d/c
C_1/R_n	0.2 a/c	1.38 d/c	1.22 d/c
R_2/R_n	0.90	0.02	1.4e-6
L_2/R_n	0.37 a/c	0.77 d/c	2.3 d/c
R_3/R_n	—	1.31	2.06
L_3/R_n	—	0.07 d/c	0.05 d/c
C_3/R_n	—	0.32 d/c	0.40 d/c
R_4/R_n	—	1.04	1.12
L_4/R_n	—	0.28 d/c	0.29 d/c

$R_n = \pi a^2 \rho_0 c / N$; ρ_0 = density of the plate material.

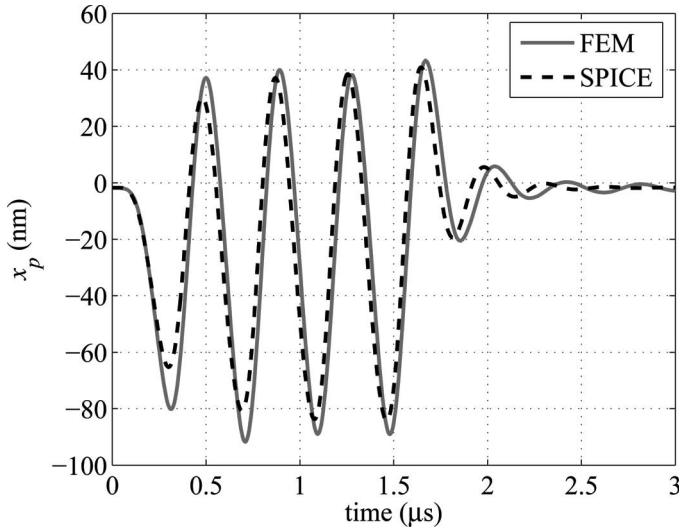


Fig. 7. A 2-cycle 95-V peak cosine burst at 1.3 MHz is applied to a capacitive micromachined ultrasonic transducer (CMUT) cell under water loading. The effect of the atmospheric pressure (100 kPa) is taken into account ($a = 300 \mu\text{m}$, $t_m = 100 \mu\text{m}$, $t_g = 100 \text{nm}$, $t_i = 200 \text{nm}$).

by causing charge trapping in the insulation layer [5], [29] and drifting of the resonance frequency of the plate [30].

For continuous wave applications, it is possible to use an excitation voltage, $V(t)$, at half of the operating frequency without a dc bias to excite CMUTs [31], [32]:

$$V(t) = V_{\max} \cos\left(\frac{\omega}{2} t\right), \quad (2)$$

where V_{\max} is the peak voltage and ω is the operating frequency. The force exerted on the plate, f_R , will be proportional to

$$f_R \propto V^2(t) = \frac{V_{\max}^2}{2} [1 + \cos(\omega t)]. \quad (3)$$

As seen in (3), $V^2(t)$ includes a dc term that will naturally form a static force at the operating frequency.

B. Determination of CMUT Dimensions

We start by assuming that the peak drive voltage is limited. The thickness of the insulation layer, t_i , is chosen such that the insulation withstands the peak voltage during the operation. For a maximum operating voltage of 100 V, the insulation layer is chosen as silicon dioxide¹ with a thickness of 200 nm.

Let us assume that the target operating frequency is 3 MHz and we use an array configuration of 7 cells. Increasing the radiation resistance seen by the CMUT array increases the power delivered to the medium [34]. Therefore, at the operating frequency we wish to maximize the radiation resistance, which is maximum at $ka = 3.75$ for

¹The theoretical dielectric strength of silicon dioxide is $\sim 1000 \text{ V}/\mu\text{m}$ [33].

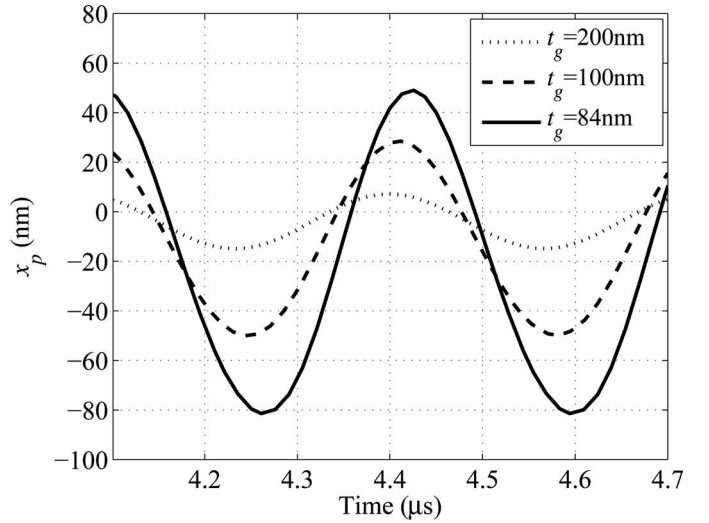


Fig. 8. The center displacement of the plate for different t_g values under a continuous 100-V peak 1.5-MHz sinusoidal signal ($a = 298.5 \mu\text{m}$, $t_m = 130 \mu\text{m}$, $t_i = 100 \text{nm}$).

an array of 7 cells, as seen in Fig. 6. Hence, the plate radius maximizing the radiation resistance at 3 MHz is $298 \mu\text{m}$. The CMUT plate must resonate at the desired operating frequency to maximize the displacement. Using the circuit model, t_m is found to be $130 \mu\text{m}$.

To determine t_g , a 100-V peak continuous wave signal at half of the resonance frequency (1.5 MHz) is applied to the circuit model. t_g is reduced until the center of the oscillating plate is about to touch the substrate. As seen in Fig. 8, at $t_g = 84 \text{nm}$, the center peak displacement of the plate reaches 80 nm. At this point, the resonance frequency shifts because of the spring-softening effect [35]. To compensate for the spring softening, the thickness of the plate is slightly increased and the last step is repeated. After a few iterations, we find $t_m = 135 \mu\text{m}$ and $t_g = 80 \text{nm}$.

For a target operating frequency and an available peak voltage, the procedure for designing a high-power CMUT is as follows:

- 1) Choose the minimum insulation layer thickness, t_i , maintaining a safe operation for a chosen maximum drive voltage.
- 2) Choose the plate radius, a , providing the maximum radiation impedance at the operating frequency.
- 3) Find the plate thickness, t_m , required for a resonance at the given operating frequency.
- 4) Choose a large gap, t_g , and then reduce the gap step by step until the plate is about to touch the substrate in the positive force cycles.
- 5) If resonance frequency shifts, repeat the previous two steps for a fine adjustment.

Table III lists the design parameters for continuous 3-MHz operation. As seen from the table, the CMUT operating at the peak of the radiation impedance provides the maximum pressure with a relatively low second harmonic.

TABLE III. DESIGN COMPARISONS AT 3 MHz.

a (μm)	ka	t_m (μm)	t_g (nm)	x_{p-p} (nm)	Surface pressure (p-p, MPa)	2nd harmonic (dBc)	Power/area (W/mm ²)
20	0.25	1.18	280	331	1.42	-14.5	1.08
50	0.62	6.2	145	149	1.43	-6.7	1.14
100	1.25	16	144	186	1.66	-8.1	1.6
298	3.75	135	80	111	2.55	-23	1.88
360	4.52	190	84	105	2.03	-25	1.5

$t_i = 200$ nm; $N = 7$; 100 V_p.

TABLE IV. DESIGN PARAMETERS FOR 1, 5, 10, AND 15 MHz.

Operating frequency (MHz)	1	5	10	15
Plate radius, a (μm)	895	179	89.5	59.6
Plate thickness, t_m (μm)	400	76	37	23
Gap height, t_g (nm)	138	65	45	40
Surface pressure (MPa)	1.45	3	4.1	4.8

$ka = 3.75$; $t_i = 200$ nm; $N = 7$; 100 V_p.

The available input voltage changes the results drastically. When the available voltage is increased to 200 V ($t_i = 400$ nm), the surface pressure reaches 3.5 MPa with harmonics at -27 dBc for the optimum design.

The procedure is also applied to operating frequencies of 1, 5, 10, and 15 MHz at 100 V maximum available voltage. CMUT dimensions for each design are given in Table IV.

IV. FABRICATION

For the fabrication of a high-power CMUT, we utilized anodic wafer bonding technology. Anodic bonding is used to bond a silicon wafer to a borosilicate wafer using proper pressure, electric field, and temperature. We defined the cavity of the CMUTs on the silicon side. The microfabrication process on the silicon side starts with a 76.2-mm (3-in), highly doped, double-side-polished silicon wafer. The microfabrication process is shown in Fig. 9. High conductivity of this wafer serves as one of the electrodes of the CMUTs. The thickness of the silicon wafer determines the thickness of the CMUT plate, which is 92 μm in this case. First, a 450-nm insulation layer of silicon oxide is thermally grown in a diffusion furnace. The silicon wafer is kept in the furnace at 1050°C for one hour in the presence of adequate water vapor. Second, 100 nm of silicon oxide is etched using a reactive ion etching (RIE) reactor to create the cavities. As the final process on the silicon side, the silicon oxide at the back side of the silicon wafer is etched away using the RIE reactor.

Having completed the plate side, the substrate side is fabricated on a 3.2-mm-thick 101.6-mm (4-in) borosilicate wafer. The substrate wafer is chosen to be quite thick to maintain a rigid substrate. Because the smoothness of the borosilicate surface is critical for the success of the anodic bonding, the substrate electrode is buried on the glass wafer. An image reversal photoresist (AZ5214E, Clari-

ant Corp., Muttentz, Switzerland) is used for the lift-off process. Before the evaporation of the gold electrode, the glass is etched approximately by the thickness of gold to be evaporated. As the substrate electrode, 15 nm of titanium and 85 nm of gold are deposited by thermal evaporation. The borosilicate and silicon wafers are cleaned at 120°C in piranha etch (1:3 H₂O₂:H₂SO₄) for 15 min before the bonding process. The prepared wafers are then anodically bonded (Applied Microengineering Ltd., Oxfordshire, UK). The current passing during the bonding process is limited to prevent dielectric breakdown, because a bonding voltage up to 1000 V is utilized.

Because the borosilicate wafer is larger than the silicon wafer, the substrate electrical contacts are made at the

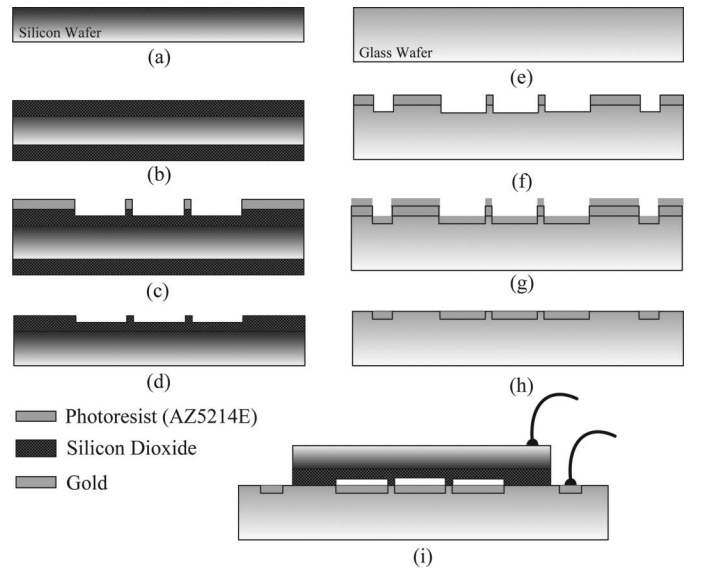


Fig. 9. Fabrication steps: (a) conductive silicon wafer, (b) thermal oxidation, (c) lithography and oxide etching for cavities, (e) borosilicate glass wafer, (f) lithography and glass etching for bottom electrode, (g) Ti/Au evaporation, (h) cleaning, and (i) anodic bonding and lead wire connection.

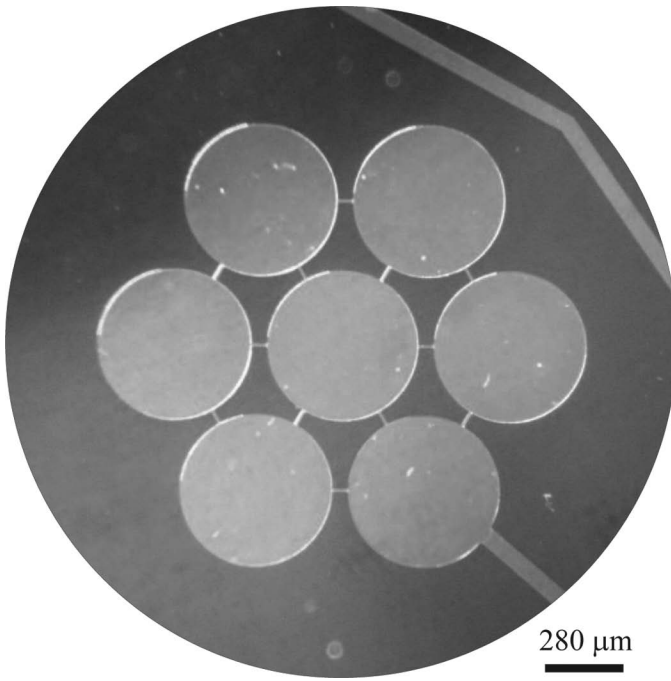


Fig. 10. A view of the capacitive micromachined ultrasonic transducer (CMUT) array from the glass side.

exposed gold electrodes on the surface of the borosilicate wafer. Electrical contacts are made using a silver conductive epoxy (Eccobond 83C, Emerson & Cumming Specialty Polymer, Billerica, MA). A microscope view of the completed device is seen in Fig. 10.

V. EXPERIMENTAL RESULTS AND DISCUSSION

The setup in Fig. 11 is used for characterizing the transmit mode of operation of the fabricated CMUTs.

The tested CMUT element's properties are given in Table V. The element consists of 7 CMUT cells and the total capacitance, including the paths, is measured as 103 pF.

Immersion experiments were done in a vegetable oil tank. Signal generator output is amplified by using an ENI 240L 40W class-A linear power amplifier (Electronic Navigation Industries, Rochester, NY). The amplifier has a fixed nominal gain of 50 dB. The amplified 5-cycle cosine burst signal at 1.44 MHz is applied to the transducer element. An HGL-200 calibrated hydrophone (Onda Corp., Sunnyvale, CA) is placed 1 cm away from the transducer surface. The AH-2010 preamplifier (Onda Corp.) is connected to the hydrophone with an Onda AR-AMAF connector. The measured signal is first corrected using hydrophone calibration data in frequency domain and then corrected for the diffraction and attenuation losses² to obtain the pressure generated on the radiation resistance at the surface. This pressure is further modified using the radiation impedance given in Fig. 6 to obtain the total pressure on the surface of the transducer. The

²Attenuation in sunflower oil, $\alpha = 5.68e^{-12} \text{ m}^{-1} \cdot \text{Hz}^{1.85}$ [36].

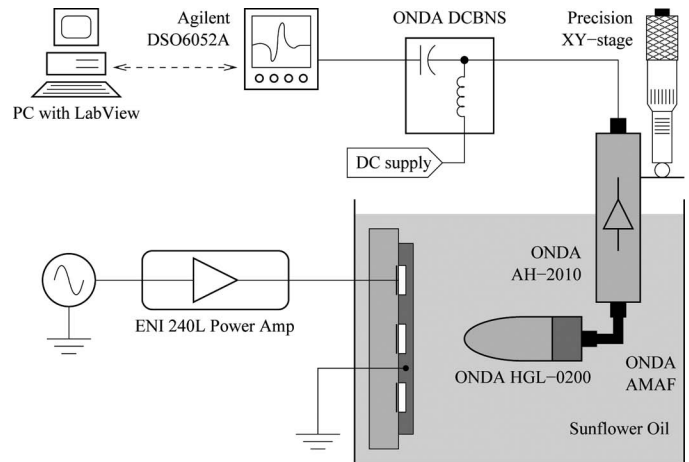


Fig. 11. Experimental setup.

TABLE V. THE PARAMETERS OF THE TESTED CAPACITIVE MICROMACHINED ULTRASONIC TRANSDUCERS (CMUT) ON A GLASS WAFER.

Plate radius, a	280 μm
Center-to-center distance, d	620 μm
Plate thickness, t_m	92 μm
Insulation layer thickness, t_i	SiO ₂ , 350 nm
Gap height, t_g	110 nm

latter modification is exact for the fundamental component at 2.88 MHz, but it does not include the effect of CMUT mechanical circuit effects, particularly the effect of plate mass, on harmonics. Therefore, the actual harmonic amplitudes in the surface pressure differ from our estimation. Because the signal has low harmonic content (second harmonic < -25 dBc), the contribution of harmonics are insignificant. The measured surface pressures for the applied peak voltages are given in Fig. 12.

For a peak voltage of 125 V, 1.8 MPa peak-to-peak pressure with -28 dBc second harmonic is measured at the transducer surface (Fig. 13). Because the load impedance of the CMUT is directly connected to the power amplifier, this voltage is measured as the maximum applicable voltage. The SPICE model predicts 1.87 MPa peak-to-peak surface pressure for the same peak voltage and the pressure can be increased up to 2.5 MPa with a maximum peak voltage of 145 V. On the other hand, 1 MPa with -32 dBc second harmonic is measured for a peak voltage of 100 V. The normalized frequency spectrum of the surface pressure for the applied peak voltages is shown in Fig. 14.

VI. CONCLUSIONS

The behavior of a fluid-loaded CMUT array can be simulated within seconds by creating the proposed circuit model in a SPICE simulator. Furthermore, the circuit can be used as a CMUT front-end IC test bench to optimize the IC's performance before fabrication.

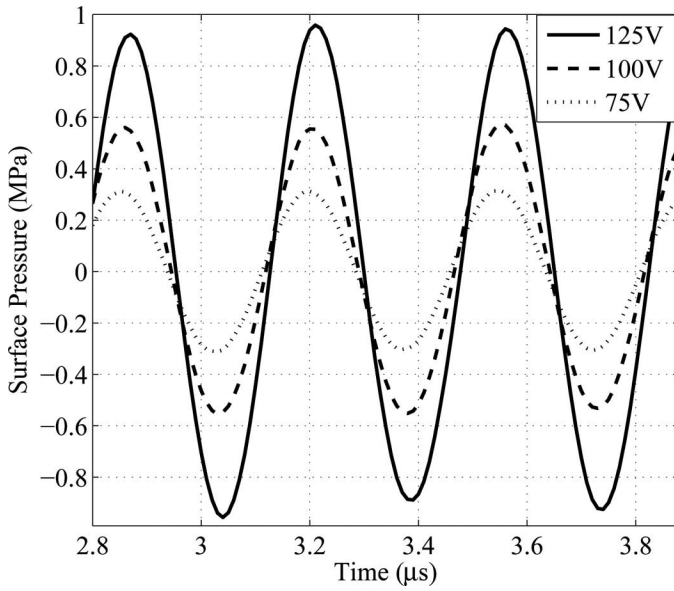


Fig. 12. Measured surface pressures for different peak voltages. The drive voltage is 1.44 MHz. The fundamental component of the pressure signal is 2.88 MHz.

Higher radiation impedance improves the transducer's performance. For the given voltage and for the given total transducer area, the CMUT cell radius should be chosen to maximize the radiation resistance at the operating frequency to get higher power. This requirement results in a large cell size. To maintain the resonance frequency, the thickness of the plate must be increased. An optimized CMUT cell has a rather thick plate compared with a conventional cell size.

The plate moves symmetrically in both directions around a stable deflection point. At the optimum operation, the center of the plate makes a full swing, almost touching the substrate, making the peak-to-peak swing considerably greater than the gap height.

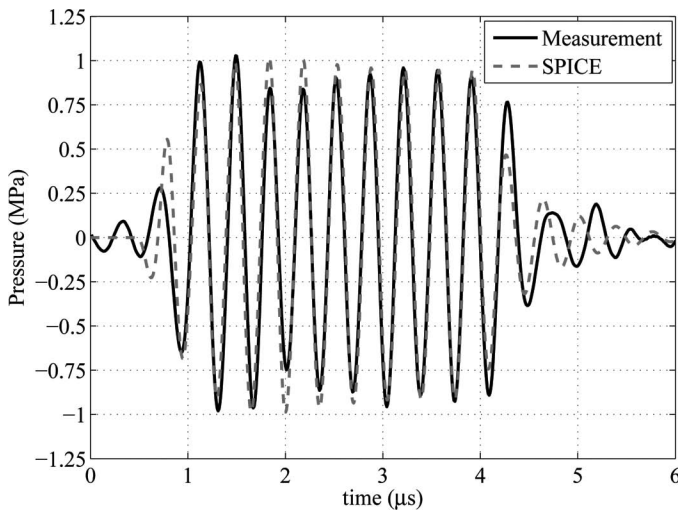


Fig. 13. A 5-cycle 125-V peak cosine burst at 1.44 MHz is applied to the capacitive micromachined ultrasonic transducer (CMUT) element. The calculated surface pressure is compared with the pressure obtained from the SPICE model.

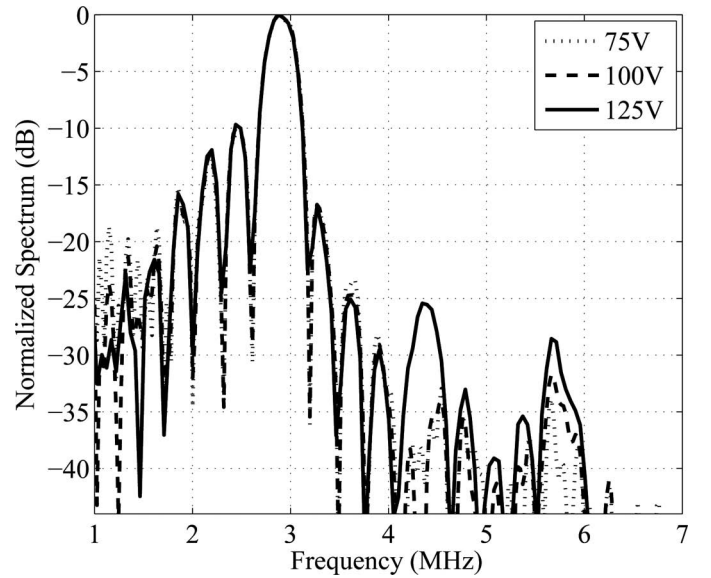


Fig. 14. Normalized frequency spectrum of the surface pressure for different peak voltages.

VII. APPENDIX

In this section, the expressions [23] for calculating the parameters of the equivalent circuit shown in Fig. 2 are given.

The electrical attraction force, f_R :

$$f_R(t) = \sqrt{5} \frac{C_0 V^2(t)}{4x_P(t)} \left[\frac{t_{ge}}{t_{ge} - x_P(t)} - \frac{\tanh^{-1}\left(\sqrt{\frac{x_P(t)}{t_{ge}}}\right)}{\sqrt{\frac{x_P(t)}{t_{ge}}}} \right], \quad (4)$$

where $C_0 = \varepsilon_0 \pi a^2 / t_{ge}$, $t_{ge} = t_g + t_i / \varepsilon_i$ is the equivalent gap height, and ε_i is the relative permittivity of the plate material.

The force, F_b , exerted by the atmospheric pressure, P_0 :

$$F_b = \frac{\sqrt{5}}{3} P_0 \pi a^2. \quad (5)$$

Inductance representing the mass of the plate:

$$L_{Rm} = \rho t_m \pi a^2. \quad (6)$$

Capacitance representing the compliance of the plate:

$$C_{Rm} = 1.8 \left[\frac{(1 - \sigma^2) a^2}{16 \pi Y_0 t_m^3} \right], \quad (7)$$

where σ and Y_0 are the Poisson's ratio and Young's modulus of the plate material, respectively. The nonlinear equations for the current sources in the model are

$$i_c = C_0 \frac{dV(t)}{dt} \left[\frac{\tanh^{-1}\left(\sqrt{\frac{x_P(t)}{t_{ge}}}\right)}{\sqrt{\frac{x_P(t)}{t_{ge}}}} - 1 \right] \quad (8)$$

$$i_{\text{vel}} = \frac{C_0 V(t)}{2x_p(t)} \frac{dx_p(t)}{dt} \left[\frac{t_{\text{ge}}}{t_{\text{ge}} - x_p(t)} - \frac{\tanh^{-1} \left(\sqrt{\frac{x_p(t)}{t_{\text{ge}}}} \right)}{\sqrt{\frac{x_p(t)}{t_{\text{ge}}}}} \right]. \quad (9)$$

REFERENCES

- [1] I. Ladabaum, X. Jin, H. T. Soh, A. Atalar, and B. T. Khuri-Yakub, "Surface micromachined capacitive ultrasonic transducers," *IEEE Trans. Ultrason. Ferroelectr. Freq. Control*, vol. 45, no. 3, pp. 678–690, 1998.
- [2] R. O. Guldiken, J. McLean, and F. L. Degertekin, "CMUTs with dual-electrode structure for improved transmit and receive performance," *IEEE Trans. Ultrason. Ferroelectr. Freq. Control*, vol. 53, no. 2, pp. 483–491, 2006.
- [3] R. O. Guldiken, J. Zahorian, F. Y. Yamaner, and F. L. Degertekin, "Dual-electrode CMUT with non-uniform membranes for high electromechanical coupling coefficient and high bandwidth operation," *IEEE Trans. Ultrason. Ferroelectr. Freq. Control*, vol. 56, no. 6, pp. 1270–1276, 2009.
- [4] J. Zahorian, M. Hochman, T. Xu, S. Satir, G. Gorun, M. Karaman, and F. L. Degertekin, "Monolithic CMUT-on-CMOS integration for intravascular ultrasound applications," *IEEE Trans. Ultrason. Ferroelectr. Freq. Control*, vol. 58, no. 12, pp. 2659–2667, 2011.
- [5] S. Olcum, F. Y. Yamaner, A. Bozkurt, H. Köymen, and A. Atalar, "Deep collapse operation of capacitive micromachined ultrasonic transducers," *IEEE Trans. Ultrason. Ferroelectr. Freq. Control*, vol. 58, no. 11, pp. 2475–2483, 2011.
- [6] S. Lani, S. Satir, G. Gurun, K. G. Sabra, and F. L. Degertekin, "High frequency ultrasonic imaging using thermal mechanical noise recorded on capacitive micromachined transducer arrays," *Appl. Phys. Lett.*, vol. 99, no. 22, pp. 103–224, Nov. 2011.
- [7] K. K. Park, H. Lee, M. Kupnik, and B. T. Khuri-Yakub, "Fabrication of capacitive micromachined ultrasonic transducers via local oxidation and direct wafer bonding," *J. Microelectromech. Syst.*, vol. 20, no. 1, pp. 95–103, 2011.
- [8] A. Logan, L. L. P. Wong, and J. T. W. Yeow, "A 1-D capacitive micromachined ultrasonic transducer imaging array fabricated with a silicon-nitride-based fusion process," *IEEE/ASME Trans. Mechatronics*, vol. 16, no. 5, pp. 861–865, 2011.
- [9] D. S. Lin, X. Zhuang, S. H. Wong, M. Kupnik, and B. T. Khuri-Yakub, "Encapsulation of capacitive micromachined ultrasonic transducers using viscoelastic polymer," *J. Microelectromech. Syst.*, vol. 19, no. 6, pp. 1341–1351, 2010.
- [10] I. O. Wygant, N. S. Jamal, H. J. Lee, A. Nikoozadeh, Ö. Oralkan, M. Karaman, and B. T. Khuri-Yakub, "An integrated circuit with transmit beamforming flip-chip bonded to a 2-D CMUT array for 3-D ultrasound imaging," *IEEE Trans. Ultrason. Ferroelectr. Freq. Control*, vol. 56, no. 10, pp. 2145–2156, 2009.
- [11] S. Vaithilingam, T.-J. Ma, Y. Furukawa, I. O. Wygant, X. Zhuang, A. De la Zerda, O. Oralkan, A. Kamaya, S. S. Gambhir, R. B. Jeffrey Jr., and B. T. Khuri-Yakub, "Three-dimensional photoacoustic imaging using a two-dimensional CMUT array," *IEEE Trans. Ultrason. Ferroelectr. Freq. Control*, vol. 56, no. 11, pp. 2411–2419, 2009.
- [12] C. H. Seo, D. N. Stephens, J. Cannata, A. Dentinger, F. Lin, S. Park, D. Wildes, K. E. Thomenius, P. Chen, T. Nguyen, A. de la Rama, J. S. Jeong, A. Mahajan, K. Shivkumar, A. Nikoozadeh, O. Oralkan, U. Truong, D. J. Sahn, P. T. Khuri-Yakub, and M. O'Donnell, "The feasibility of using thermal strain imaging to regulate energy delivery during intracardiac radio-frequency ablation," *IEEE Trans. Ultrason. Ferroelectr. Freq. Control*, vol. 58, no. 7, pp. 1406–1417, 2011.
- [13] H. J. Lee, K. K. Park, M. Kupnik, O. Oralkan, and B. T. Khuri-Yakub, "Chemical vapor detection using a capacitive micromachined ultrasonic transducer," *Anal. Chem.*, vol. 83, no. 24, pp. 9314–9320, 2011.
- [14] I. O. Wygant, M. Kupnik, J. C. Windsor, W. M. Wright, M. S. Wochner, G. G. Yaralioglu, M. F. Hamilton, and B. T. Khuri-Yakub, "50 kHz capacitive micromachined ultrasonic transducers for generation of highly directional sound with parametric arrays," *IEEE Trans. Ultrason. Ferroelectr. Freq. Control*, vol. 56, no. 1, pp. 193–203, 2009.
- [15] F. L. Degertekin, R. O. Guldiken, and M. Karaman, "Annular-ring CMUT arrays for forward-looking IVUS: Transducer characterization and imaging," *IEEE Trans. Ultrason. Ferroelectr. Freq. Control*, vol. 53, no. 2, pp. 474–482, 2006.
- [16] J. E. Kennedy, G. R. ter Haar, and D. Cranston, "High intensity focused ultrasound: Surgery of the future?" *Br. J. Radiol.*, vol. 76, no. 909, pp. 590–599, 2003.
- [17] B. T. Khuri-Yakub and O. Oralkan, "Capacitive micromachined ultrasonic transducers for medical imaging and therapy," *J. Micro-mech. Microeng.*, vol. 21, no. 5, 2011.
- [18] S. H. Wong, R. D. Watkins, M. Kupnik, K. B. Pauly, and B. T. Khuri-Yakub, "Feasibility of MR-temperature mapping of ultrasonic heating from a CMUT," *IEEE Trans. Ultrason. Ferroelectr. Freq. Control*, vol. 55, no. 4, pp. 811–818, 2008.
- [19] S. H. Wong, M. Kupnik, R. D. Watkins, K. Butts-Pauly, and B. T. Khuri-Yakub, "Capacitive micromachined ultrasonic transducers for therapeutic ultrasound applications," *IEEE Trans. Biomed. Eng.*, vol. 57, no. 1, pp. 114–123, 2010.
- [20] M. Wang, J. Chen, X. Cheng, J.-C. Cheng, and P.-C. Li, "Design and test of a monolithic ultrasound-image-guided HIFU device using annular CMUT rings," in *Proc. IEEE Ultrasonics Symp.*, 2008, pp. 459–462.
- [21] S. Wong, M. Kupnik, K. Pauly, and B. Khuri-Yakub, "Capacitive micromachined ultrasonic transducer (CMUT) for MR-guided non-invasive therapeutic ultrasound applications," in *Int. Solid-State Sensors, Actuators, and Microsystems Conf.*, 2009, pp. 354–357.
- [22] J. McLean, R. O. Guldiken, and F. L. Degertekin, "CMUTs with dual electrode structure for improved transmit and receive performance," in *Proc. IEEE Ultrasonics Symp.*, 2004, pp. 501–504.
- [23] H. Köymen, A. Atalar, E. Aydogdu, C. Kocabas, K. Oguz, S. Olcum, A. Ozguruk, and A. Unlugedik, "An improved lumped element nonlinear circuit model for a circular CMUT cell," submitted for publication.
- [24] A. Bozkurt, I. Ladabaum, A. Atalar, and B. T. Khuri-Yakub, "Theory and analysis of electrode size optimization for capacitive microfabricated ultrasonic transducers," *IEEE Trans. Ultrason. Ferroelectr. Freq. Control*, vol. 46, no. 6, pp. 1364–1374, 1999.
- [25] H. K. Oguz, S. Olcum, M. N. Senlik, V. Tas, A. Atalar, and H. Köymen, "Nonlinear modeling of an immersed transmitting capacitive micromachined ultrasonic transducer for harmonic balance analysis," *IEEE Trans. Ultrason. Ferroelectr. Freq. Control*, vol. 57, no. 2, pp. 438–447, 2010.
- [26] H. Köymen, M. N. Senlik, A. Atalar, and S. Olcum, "Parametric linear modeling of circular CMUT membranes in vacuum," *IEEE Trans. Ultrason. Ferroelectr. Freq. Control*, vol. 54, no. 6, pp. 1229–1239, 2007.
- [27] M. N. Senlik, S. Olcum, H. Köymen, and A. Atalar, "Radiation impedance of an array of circular capacitive micromachined ultrasonic transducers," *IEEE Trans. Ultrason. Ferroelectr. Freq. Control*, vol. 57, no. 4, pp. 969–976, 2010.
- [28] A. Bozkurt, "A lumped-circuit model for the radiation impedance of a circular piston in a rigid baffle," *IEEE Trans. Ultrason. Ferroelectr. Freq. Control*, vol. 55, no. 9, pp. 2046–2052, 2008.
- [29] S. Machida, S. Migita, H. Tanaka, K. Hashiba, H. Enomoto, Y. Tadaki, and T. Kobayashi, "Analysis of the charging problem in capacitive micro-machined ultrasonic transducers," in *Proc. IEEE Ultrasonics Symp.*, 2008, pp. 383–385.
- [30] K. Midtbo and A. Ronnekleiv, "Analysis of charge effects in high frequency CMUTs," in *Proc. IEEE Ultrasonics Symp.*, 2008, pp. 379–382.
- [31] H. Oguz, S. Olcum, M. Senlik, A. Atalar, and H. Köymen, "A novel equivalent circuit model for CMUTs," in *IEEE Int. Ultrasonics Symp.*, 2009 pp. 2193–2196.
- [32] J. Zahorian, M. Hochman, S. Satir, and F. L. Degertekin, "Bias optimization of dual ring CMUT arrays for forward looking IVUS applications," in *IEEE Int. Ultrasonics Symp.*, 2010, pp. 447–450.
- [33] N. Klein and H. Gafni, "The maximum dielectric strength of thin silicon oxide films," *IEEE Trans. Electron Devices*, vol. 13, no. 2, pp. 281–289, 1966.
- [34] M. Senlik, S. Olcum, H. Köymen, and A. Atalar, "Bandwidth, power and noise considerations in airborne CMUTs," in *IEEE Int. Ultrasonics Symp.*, 2009, pp. 438–441.
- [35] F. Hunt, *Electroacoustics: The Analysis of Transduction and its Historical Background*, 2nd ed. Cambridge, MA: Harvard University Press, 1982.
- [36] R. Chanamai and D. J. McClements, "Ultrasonic attenuation of edible oils," *J. Am. Oil Chem.*, vol. 75, pp. 1447–1448, 1998.



F. Yalçın Yamaner received his B.Sc. degree from Ege University, Izmir, Turkey, in 2003 and his M.Sc. and Ph.D. degrees from Sabanci University, Istanbul, Turkey, in 2006 and 2011, respectively, all in electrical and electronics engineering. He worked as a visiting researcher at the VLSI Design and Education Center (VDEC), during the summer of 2006. He was a visiting scholar in the Micromachined Sensors and Transducers Laboratory, Georgia Institute of Technology, Atlanta, GA, in 2008. He is currently a postdoctoral associate

at Laboratory of Therapeutic Applications of Ultrasound, French National Institute of Health and Medical Research (INSERM). His current research is to develop MR-guided interstitial ultrasonic CMUT probes for thermal ablation of cancerous tumors.



Selim Olçum was born in Chicago, IL, in 1981. He received his B.S., M.S., and Ph.D. degrees in electrical engineering from Bilkent University, Ankara, Turkey, in 2003, 2005, and 2010, respectively. He worked as a guest researcher in the Semiconductor Electronics Division, National Institute of Standards and Technology, Gaithersburg, MD, during the summers of 2002 and 2003. He was a visiting scholar in the Micromachined Sensors and Transducers Laboratory, Georgia Institute of Technology, Atlanta, GA, in 2006. He was an instructor in the Electrical and Electronics Engineering Department at Bilkent University for six months in 2011. He is currently a postdoctoral associate in the Department of Biological Engineering and Koch Institute for Integrative Cancer Research at the Massachusetts Institute of Technology, Cambridge, MA. His dissertation work was focused on developing high-performance micromachined ultrasonic transducers. His current research focus at MIT is to develop real-time techniques for biomolecular detection using micro- and nano-electromechanical devices.

Dr. Selim Olçum was a fellow of ASELSAN during his Ph.D. study.



H. Kağan Oğuz was born in Ankara, Turkey, in 1985. He received his B.S. and M.S. degrees in electrical engineering from Bilkent University, Ankara, Turkey, in 2006 and 2009, respectively. Between 2009 and 2012, he worked as an R&D engineer in the Underwater Acoustic Systems Division, Meteksan Defence Industry Inc., Ankara. Since 2009, he has been working toward his Ph.D. degree in the Electrical and Electronics Engineering Department at Bilkent University, where he is currently a research assistant. His current research

interests include the design and fabrication of underwater transducers and CMUTs.



Ayhan Bozkurt (M'91) received his B.Sc., M.Sc., and Ph.D. degrees from Bilkent University, Ankara, Turkey, in 1992, 1994, and 2000, respectively, all in electrical and electronics engineering. He is currently working as an Associate Professor in the Electronics Engineering Program, Faculty of Engineering and Natural Sciences, Sabanci University, Istanbul, Turkey. His research interests are RF circuit design, ultrasonic transducer modeling and fabrication, and high-voltage CMOS integrated circuit design.



Hayrettin Köymen received the B.Sc. and M.Sc. degrees from the Middle East Technical University (METU), Ankara, Turkey, in 1973 and 1976, respectively, and the Ph.D. degree from Birmingham University, UK, in 1979, all in electrical engineering. He worked as a faculty member in the Marine Sciences Department (Mersin) and Electrical Engineering Department (Ankara) of METU from 1979 to 1990; since 1990, he has been a professor at Bilkent University. His research activities have included underwater acoustic and

ultrasonic transducer design, acoustic microscopy, ultrasonic NDT, biomedical instrumentation, mobile communications, and spectrum management.

Prof. Köymen is a fellow of IET (formerly IEE).



Abdullah Atalar received his B.S. degree from the Middle East Technical University, Ankara, Turkey, in 1974, and his M.S. and Ph.D. degrees from Stanford University, Stanford, CA, in 1976 and 1978, respectively, all in electrical engineering. He worked at Hewlett-Packard Labs, Palo Alto, CA, in 1979. From 1980 to 1986, he was on the faculty of the Middle East Technical University as an Assistant Professor. In 1986, he joined Bilkent University as the chairman of the Electrical and Electronics Engineering Department and

served in the founding of the Department, where he is currently a Professor. In 1995, he was a Visiting Professor at Stanford University. From 1996 to 2010, he was the Provost of Bilkent University. He is presently the Rector of the same university. His current research interests include micromachined devices and microwave electronics.

Prof. Atalar was awarded the Science Award of TUBITAK in 1994. He is a Fellow of IEEE and a member of the Turkish Academy of Sciences.